Full Paper Transactions, SMiRT 28
Toronto, Canada, August 10-15, 2025

Injury Evaluation of NPP Operator During Earthquake Based on Seismic Response Analysis Model of Human Body Considering Collision

Keito Nihommatsu[1], Takenori Hida[2]

[1] Graduate Student, Ibaraki University, Ibaraki, Japan (24nm831g@vc.ibaraki.ac.jp)
[2] Associate Professor, Ibaraki University, Ibaraki, Japan (takenori.hida.mn75@vc.ibaraki.ac.jp)

ABSTRACT

When a severe accident occurs at a nuclear power plant during an earthquake, damage mitigation efforts by managers and operators are required, such as the case of the Fukushima daiichi nuclear power plant damaged by the 2011 off the Pacific coast of Tohoku Earthquake. If the managers and operators suffer injury during an earthquake, they are incapable of providing post-accident response. In fact, it is reported that many humans suffered injury due to fall and collide with objects during the shaking of the past earthquakes. Hence, in order to study human injury measures to mitigate damage at NPP, it is necessary to estimate the human behaviour during the shaking of an earthquake. In this study, we construct the seismic response analysis model of human body considering collision. Finally, we perform seismic response analyses considering the collision between humans by using two human body models to investigate the validity of the model.

INTRODUCTION

In the 2011 off the Pacific coast of Tohoku Earthquake, the severe accident was occurred at the Fukushima Daiichi Nuclear Power Plant. The managers and operators struggled to prevent further spread of the accident. As in the case of the 2011 accident at Fukushima Daiichi NPP, human control and damage mitigation efforts by managers and operators are required when accidents occur. On the other hand, there are many cases of injuries caused by human falls and collisions with objects during the shaking of the past earthquakes, such as the studies by National Research Institute of Fire and Disaster (2005) and Ikuta, et al. (2005). Hence, assuming that an accident occurs at a NPP due to a massive earthquake, it is necessary to avoid injury to the managers and operators during the shaking of an earthquake.

Based on the above background, Takada, et al. (2017) proposed that when discussing the safety of NPP during earthquake, it is extremely important to comprehensively consider the entire system, including the surrounding environment, buildings, equipment, and the people who operate and control them. Hida, et al. (2019) also stated that it is necessary to evaluate and predict human seismic response in order to assess human damage during the shaking of an earthquake. In the study, a seismic response analysis model of human body (human body model) was constructed. Furthermore, Sakuma and Hida (2023) constructed the human body model in the forward-backward direction that takes walking into account. Sato and Hida (2024) also constructed the human body model in the left-right direction.

However, collisions between human and humans or obstacles are not considered in the models. Therefore, evaluation of human damages was inadequate for situations where multiple people are staying in the same space or where there are obstacles.

In this study, the Distinct Element Method (DEM) is incorporated into the human body model to consider collisions between human and humans or obstacles.

HUMAN BODY MODEL CONSIDERING COLLISION

Human Body Model

In this study, the human body model in the forward-backward direction (Sakuma and Hida (2023)) that takes walking into account and the human body model in the left-right direction (Sato and Hida (2024)) are combined. In addition, collision between the human body and the other objects is considered.

Figure 1 shows the human body model considering collision. Figure 1 a) shows the human body model in the forward-backward direction (Sakuma and Hida (2023)) that takes walking into account, whereas figure 1 b) shows the human body model in the left-right direction (Sato and Hida (2024)). The models were constructed with a cart-type double inverted pendulum. The upper and lower pendulums correspond to the upper and lower body of the human body, respectively. The movement of the cart corresponds to the Center of Pressure (CoP) movement due to the postural control and walking. In the forward-backward direction, a dashpot and a rotating spring are installed at the hinge between the upper and lower pendulums to prevent the hip from arching backward.

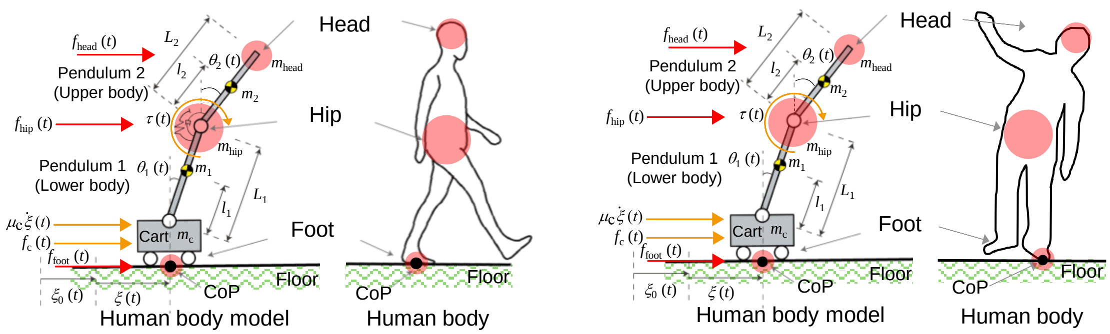

a) Human body model in the forward-backward direction (Sakuma and Hida (2023))

b) Human body model in the left-right direction (Sato and Hida (2024))

Figure 1. Human body model considering collision

In this analytical model, state feedback control system is used to maintain the human body model's standing posture. In the control system, the controlling force $f_c(t)$ and torque $\tau(t)$ are applied to the cart and hip, respectively. Figure 2 shows a block diagram of the feedback control system. Controlling force $f_c(t)$ and torque $\tau(t)$ are generated to bring the state vector $\mathbf{x}(t)$, such as the displacement of the cart, to a targeted state represented as the reference vector $\mathbf{r}$.

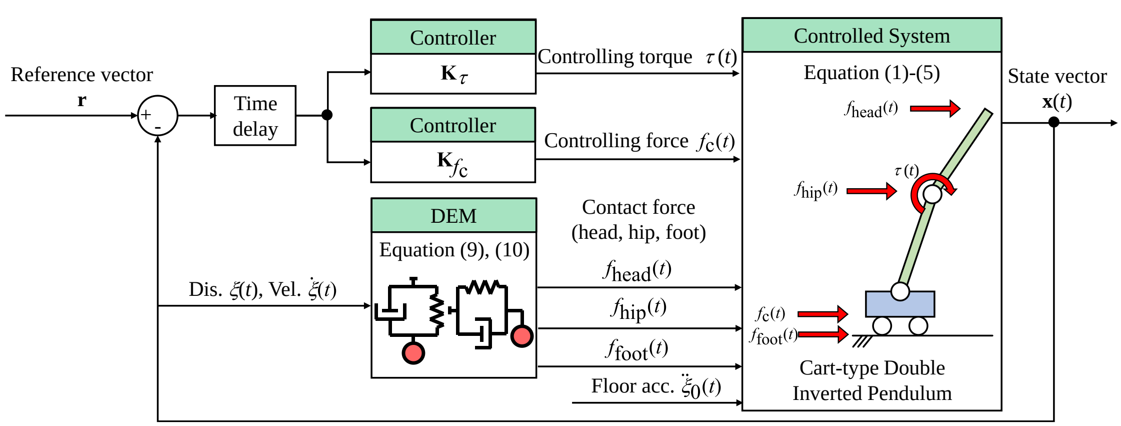

Figure 2. Block diagram of human body model considering collision

The nonlinear equations of motion of the human body model are expressed as follows.

$$\begin{aligned} &d_1\{\ddot{\xi}_0(t)+\ddot{\xi}(t)\}+d_2\ddot{\theta}_1(t)\cos\theta_1(t)+d_3\ddot{\theta}_2(t)\cos\theta_2(t)+\mu_c\dot{\xi}(t)\\ &=d_2\{\dot{\theta}_1(t)\}^2\sin\theta_1(t)+d_3\{\dot{\theta}_2(t)\}^2\sin\theta_2(t)+w_f(t)f_c(t)+f_{foot}(t) \end{aligned} \tag{1}$$

$$\begin{aligned} &d_2\cos\theta_1(t)\{\ddot{\xi}_0(t)+\ddot{\xi}(t)\}+d_4\ddot{\theta}_1(t)+d_5\ddot{\theta}_2(t)\cos\theta_1(t)\cos\theta_2(t)-\tau_p(t)-\mu_p\{\dot{\theta}_2(t)-\dot{\theta}_1(t)\}\\ &=d_7\sin\theta_1(t)+d_5\{\dot{\theta}_2(t)\}^2\cos\theta_1(t)\sin\theta_2(t)+d_6\{\dot{\theta}_1(t)\}^2\sin\theta_1(t)\cos\theta_1(t)-\tau(t)+f_{hip}(t)L_1 \end{aligned} \tag{2}$$

$$\begin{aligned} &d_3\cos\theta_2(t)\{\ddot{\xi}_0(t)+\ddot{\xi}(t)\}+d_5\ddot{\theta}_1(t)\cos\theta_1(t)\cos\theta_2(t)+d_8\ddot{\theta}_2(t)+\tau_p(t)+\mu_p\{\dot{\theta}_2(t)-\dot{\theta}_1(t)\}\\ &=d_9\{\dot{\theta}_2(t)\}^2\sin\theta_2(t)\cos\theta_2(t)+d_{10}\sin\theta_2(t)+\tau(t)+d_5\{\dot{\theta}_1(t)\}^2\sin\theta_1(t)\cos\theta_2(t)-f_{hip}(t)L_2+f_{head}(t)L_2 \end{aligned} \tag{3}$$

$$d_{11}\ddot{\xi}_{hip}(t)+d_3\ddot{\theta}_2(t)\cos\theta_2(t)=d_3\{\dot{\theta}_2\}^2\sin\theta_2(t)+f_{hip}(t) \tag{4}$$

$$m_{head}\ddot{\xi}_{head}(t)=f_{head}(t) \tag{5}$$

Where, $\xi_0(t)$ is the absolute displacement of the floor at time t. $\xi(t)$, $\xi_{hip}(t)$, and $\xi_{head}(t)$ are the relative displacements of the cart, hip, and head to the floor, respectively. m_{head} is the mass of head. L_1 and L_2 are the total lengths of the lower and upper pendulums. $\theta_1(t)$ and $\theta_2(t)$ are the angles with respect to the vertical line of the lower and upper pendulum. μ_c is the viscosity coefficient of the cart. μ_p is the viscosity coefficient of the hip. $\tau_p(t)$ is the torque generated by the spring installed in the human body model in the forward-backward direction to prevent excessive back bending of the upper body. It is expressed by the following equation (6). $w_f(t)$ is the limiting factor for the control force on the cart, taking into account the maximum human step-out width. $f_c(t)$ is the control force applied to the cart. $\tau(t)$ is the control torque applied to the hinge between the lower and upper pendulum.

$$\tau_p(t)=\begin{cases} 0 & \left(0\leq\left(\theta_2(t)-\theta_1(t)\right)\right) \\ k_p\{\theta_2(t)-\theta_1(t)\} & \left(0>\left(\theta_2(t)-\theta_1(t)\right)\right) \end{cases} \tag{6}$$

Where, k_p is the stiffness of the attached spring between the lower and upper pendulum.
Note that $d_1 \sim d_{11}$ in equations (1)-(5) can be expressed as follows.

$$d_1=m_c+m_1+m_{hip}+m_2+m_{head} \quad d_2=m_1l_1+m_{hip}L_1+m_2L_1+m_{head}L_1 \quad d_3=m_2l_2+m_{head}L_2$$

$$d_4=\{\cos\theta_1(t)\}^2\{m_1{l_1}^2+{L_1}^2\left(m_{hip}+m_2+m_{head}\right)\}+J_1 \quad d_5=(m_2l_2+m_{head}L_2)L_1 \quad d_6=m_1{l_1}^2+{L_1}^2\left(m_{hip}+m_2+m_{head}\right)$$

$$d_7=\{m_1l_1+L_1\left(m_{hip}+m_2+m_{head}\right)\}g \quad d_8=\left(m_2{l_2}^2+m_{head}{L_2}^2\right)\{\cos\theta_2(t)\}^2+J_2 \quad d_9=m_2{l_2}^2+m_{head}{L_2}^2$$

$$d_{10}=(m_2l_2+m_{head}L_2)g \quad d_{11}=m_{hip}+m_2+m_{head} \tag{7}$$

Where, m_1, m_2, m_c and m_{hip} are the masses of lower pendulum, upper pendulum, the cart, and the hip, respectively. l_1 and l_2 are the heights from the lower end to the center of mass of the lower and upper pendulums. J_1 and J_2 are the rotational inertia of the lower and upper pendulums. g is the gravitational acceleration.

Human Body Model Incorporating the DEM

In this study, DEM that models contact forces between particles is used. Figure 3 shows the concept of DEM. Springs and dashpots are installed both in the normal and tangential directions. In this method, the contact force between particles is reproduced by springs and dashpots. The forces in the normal direction reproduce repulsion, whereas the forces in the tangential direction reproduce friction.

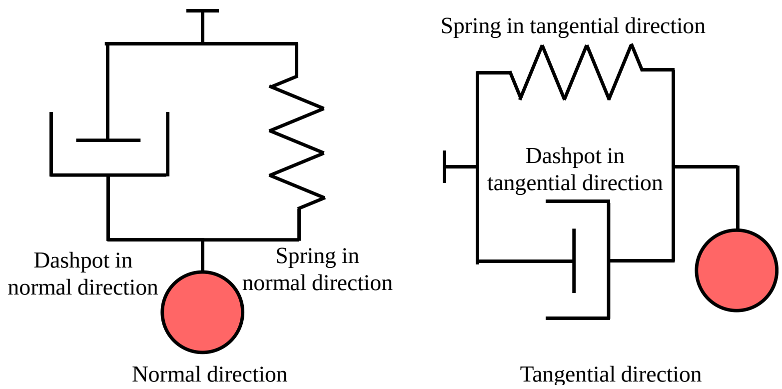

Figure 3. Concept of DEM

Particles of the DEM are installed at the head, hip, and foot of the human body model. Consequently, when the head, hip, or foot collides with other object, a contact force is generated.

Figure 4 shows collision between particles (human body and human body).

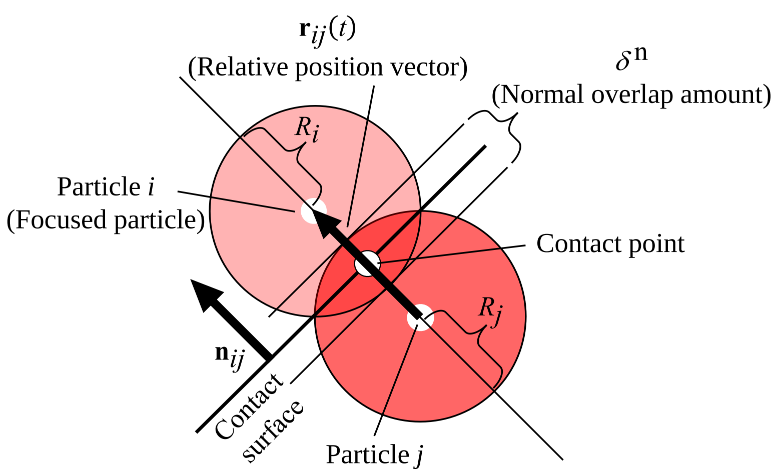

Figure 4. Collision between particles

When the following conditional equation (8) is satisfied, a collision between the particles has occurred.

$$R_i + R_j > \left| \mathbf{r}_{ij}(t) \right| \tag{8}$$

Where, R_i and R_j are the radius of particles *i* and *j*, respectively, as shown in Figure 4. $\mathbf{r}_{ij}(t)$ is the relative position vector of the center of particle *i* observed from the center of particle *j* at time *t*. When a particle collides with the other one, the contact force is generated, as given in the following equations (9) and (10).

$$\mathbf{f}^{\,\mathrm{n}}=K^{\,\mathrm{n}}\delta^{\,\mathrm{n}}\mathbf{n}_{ij}+C^{\,\mathrm{n}}\mathbf{v}^{\mathrm{n}}{}_{ji} \tag{9}$$

$$\mathbf{f}^{\,\mathrm{t}}=K^{\,\mathrm{t}}\boldsymbol{\delta}^{\,\mathrm{t}}+C^{\,\mathrm{t}}\mathbf{v}^{\mathrm{t}}{}_{ji} \tag{10}$$

Where, $\mathbf{f}^{\,\mathrm{n}}$ and $\mathbf{f}^{\,\mathrm{t}}$ are the forces in the normal and tangential directions. $K^{\,\mathrm{n}}$ and $K^{\,\mathrm{t}}$ are linear spring constants in the normal and tangential directions. $C^{\,\mathrm{n}}$ and $C^{\,\mathrm{t}}$ are linear damping coefficients in the normal and tangential directions. $\delta^{\,\mathrm{n}}$ is the normal overlap amount. $\boldsymbol{\delta}^{\,\mathrm{t}}$ is the cumulative tangential slip displacement. $\mathbf{n}_{ij}$ is the normal vector of the contact surface. $\mathbf{v}^{\mathrm{n}}{}_{ji}$ and $\mathbf{v}^{\mathrm{t}}{}_{ji}$ are the relative velocity vectors of "particle *j* observed from the side of particle *i* at the contact point" in the normal and tangential directions. $K^{\,\mathrm{n}}$, $K^{\,\mathrm{t}}$, $C^{\,\mathrm{n}}$, and $C^{\,\mathrm{t}}$ were set with reference to (Kiyono, et al. (1998)).

Figure 5 shows the collision between the particle and the surface (human body and a wall or furniture).

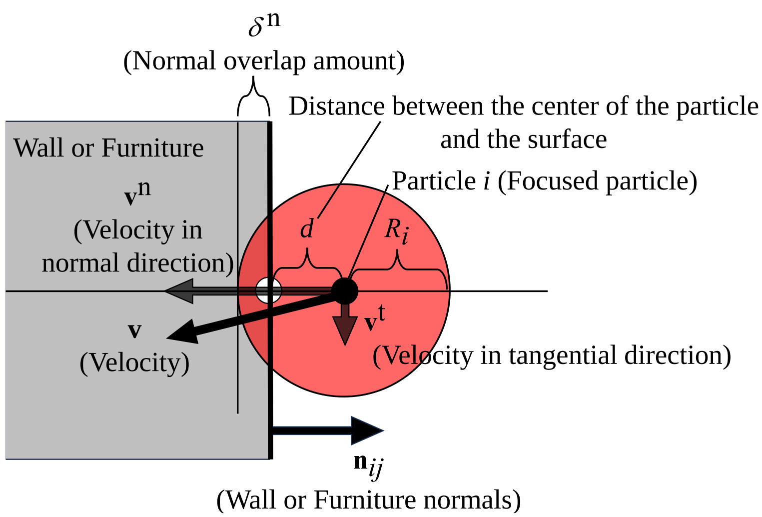

Figure 5. Collision between the particle and the surface

When the following conditional equation (11) is satisfied, a collision between the particle and the surface has occurred.

$$R_i > d \tag{11}$$

Where, R_i is the radius of particle *i*, as shown in Figure 5. *d* is the distance between the center of particle *i* and the surface. When the particle collides with the wall or furniture surface, the contact force is generated as given by equations (9) and (10) shown above.

In this study, the parts of the body considered for collision by the DEM are the head, hip, and foot. Table 1 shows the parameters set for this analysis model. Where, r_{foot}, r_{hip}, and r_{head} are the radius of the particles installed at the foot, hip, and head, respectively. In this study, the parameters of this analytical model were set with reference to the data of the human subject in the shaking table test (Hida, et al. (2019)) and the previous study (D. Gordon E. Robertson, et al. (2013), Kouchi and Mochimaru (2005)). In the shaking table test, the human subject was excited by the strong motion record observed at the Kashiwazaki-

Kariwa nuclear power plant during the Niigataken Chuetsu-oki Earthquake in 2007. Then the subject's behavior during the excitation was recorded. The human body models described above (Hida, et al. (2019), Sakuma and Hida (2023), and Sato and Hida (2024)) were constructed so as to represent the behavior of the human subject in these experiments.

Table 1: Parameters set in this analytical model

m_1	m_2	m_c	m_{hip}	m_{head}	r_{foot}	r_{hip}	r_{head}
13.0 kg	30.1 kg	1.68 kg	8.09 kg	4.15 kg	0.0338 m	0.143 m	0.0888 m

ANALYSIS RESULTS

Finally, we perform seismic response analyses considering the collision between humans by using two human body models in order to investigate the validity of the model. In this chapter, we intentionally make the human body model to collide with the other model. By colliding the two models, we examine the contact forces that occur when they collide.

For the input motion, we used a strong motion record (the Japan Meteorological Agency, 2011) observed at Shinmachi, Wakuya-cho, Miyagi Prefecture, Japan, during the 2011 off the Pacific coast of Tohoku Earthquake. Figure 6 shows the acceleration time history of input motion.

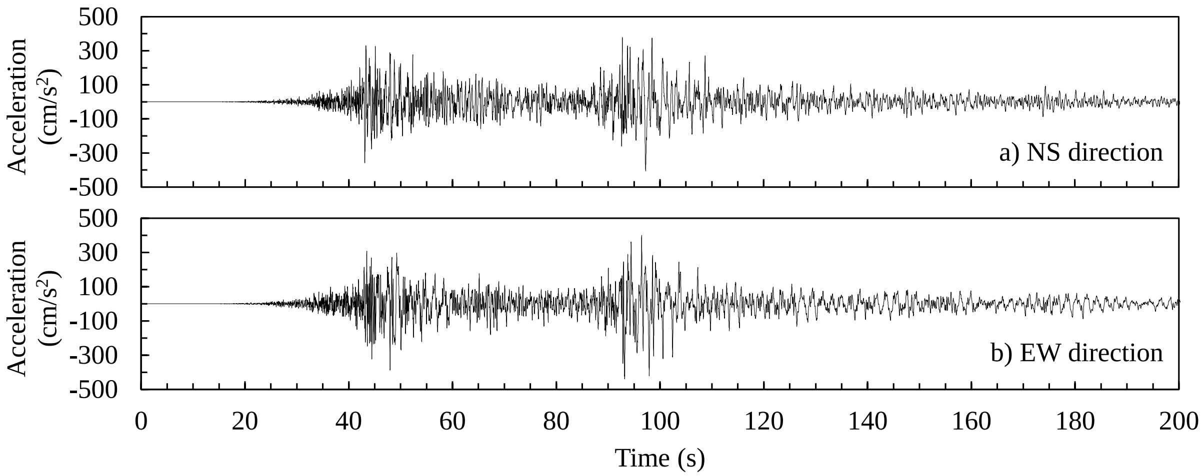

Figure 6. Acceleration time history of input motion

The seismic response analyses are performed in two cases. In Case A, two models walking on intersecting paths collide in the middle of their paths. In Case B, two models walking on the same path collide when the one passes the other. In both cases A and B, the models were assumed to initiate walking when the triaxial composite acceleration reached 60 cm/s^2. As a result, in both cases, the models started to walk at 29.7 s.

First, we perform seismic response analysis of Case A. Figure 7 shows a bird's-eye view of the analysis. In Case A, the input motion between 0 and 47 seconds were used.

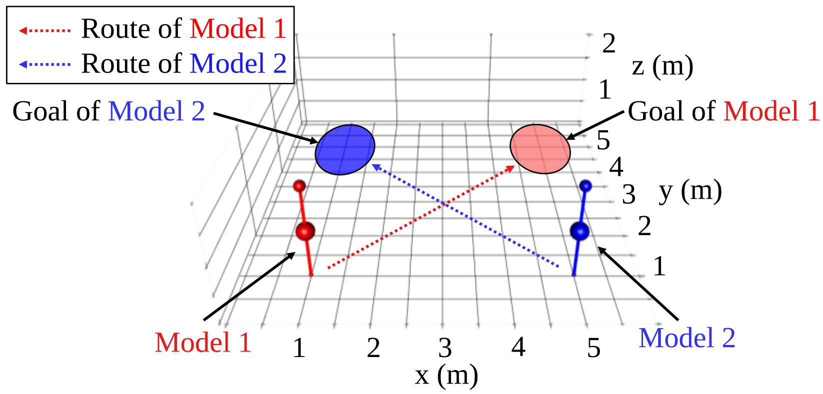

Figure 7. Overview at the situation of analysis (Case A)

The coordinate of start positions of Model 1 and Model 2 were set to (x, y) = (1 m, 1 m) and (5 m, 1 m), respectively. The coordinate of goal positions of Model 1 and Model 2 were set to (x, y) = (5 m, 5 m) and (1 m, 5 m), respectively. As a result of this setup, the two models walk toward the goal during an earthquake. Along the way, they collide with each other. The snapshots of the analytical result and the time history of the contact forces applied to Model 1 are shown in figure 8 and 9, respectively.

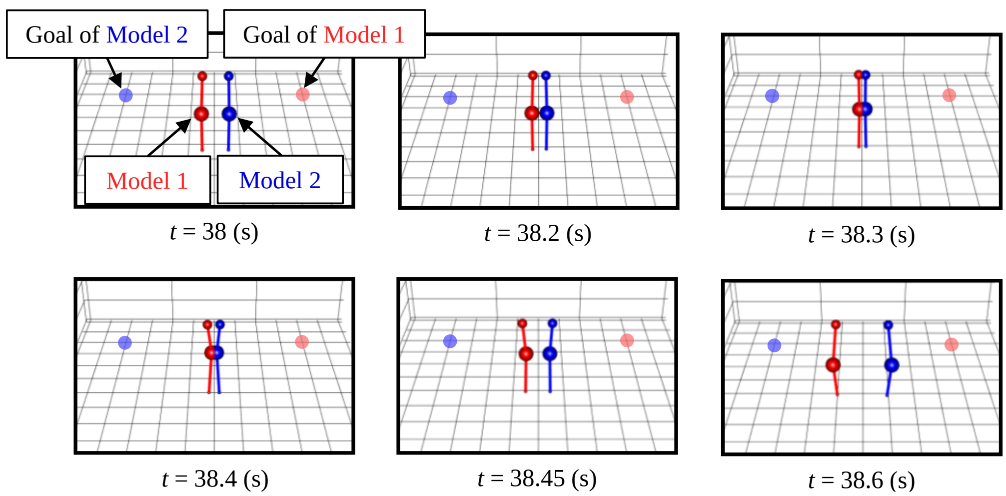

Figure 8. The snapshots of the analytical result near the time of collision (Case A)

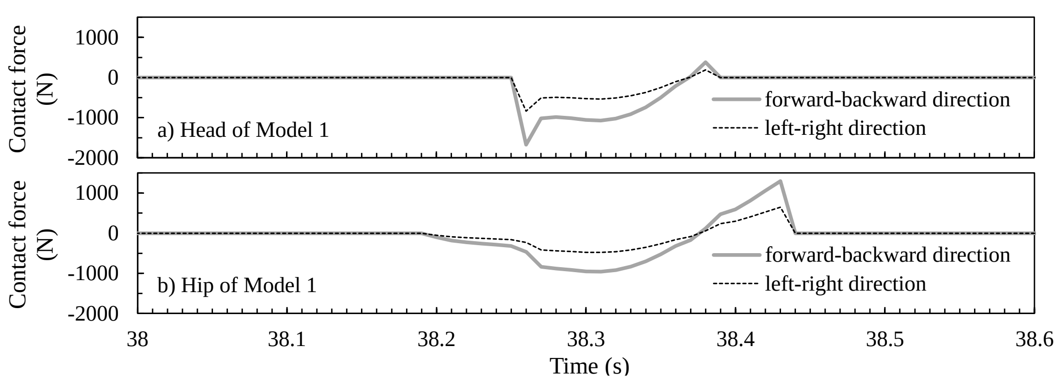

Figure 9. Time history of contact forces applied to Model 1 near the time of collision (Case A)

The contact force between two models was generated around 38.3 s. The contact points were the head and hip. First, the hips of both models collided with each other, then the heads of both models collided. As shown in figure 8, both models were facing forward at the moment of collision, so the contact force applied to both the head and the hip was larger in the forward-backward direction than in the left-right direction. Therefore, as shown in figure 8, the posture of both models was disturbed especially in the forward-backward direction after the collision. As shown in figure 9, the maximum contact forces applied to the head and hip in the forward-backward direction are 1672 N and 1296 N, respectively. These contact force values were slightly larger than those reported in previous study (Tamagawa, et al. (2011)). This is because that this study differs from the previous study. In the previous study, one of the models was kept stationary until collision, whereas in this study, both models are in motion at the time of collision. Furthermore, this study takes into account the human response to seismic shaking, which was not considered in the previous study.

Finally, we perform seismic response analysis of Case B. In this case, the input motion between 0 and 62 seconds were used. The coordinate of start positions of Model 1 and Model 2 were set to (x, y) = (1.2 m, 1 m) and (0.5 m, 0.6 m), respectively. The coordinate of goal positions of Model 1 and Model 2 were both set to (x, y) = (21 m, 21 m). As a result of this setup, the two models will each walk toward the same goal, withstanding the shaking of the earthquake. The two models collide when Model 2, which is farther from the goal at the start, overtakes Model 1. The snapshots of the analytical result and the time history of the contact forces applied to Model 1 are shown in figure 10 and 11, respectively.

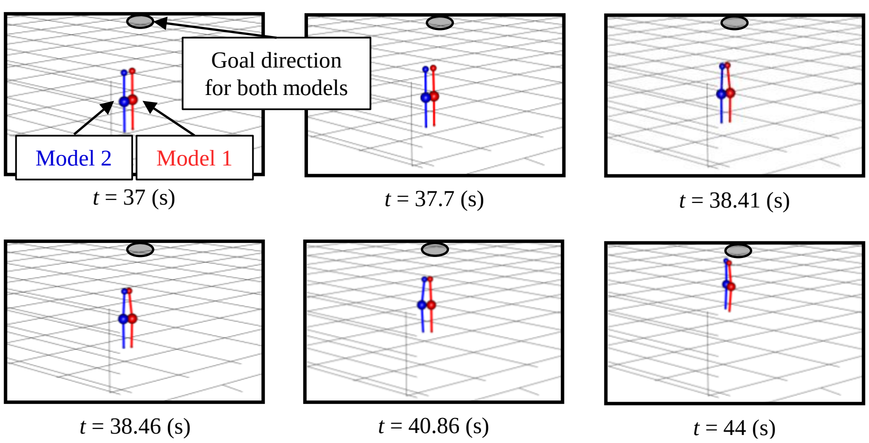

Figure 10. The snapshots of the analytical result near the time of collision (Case B)

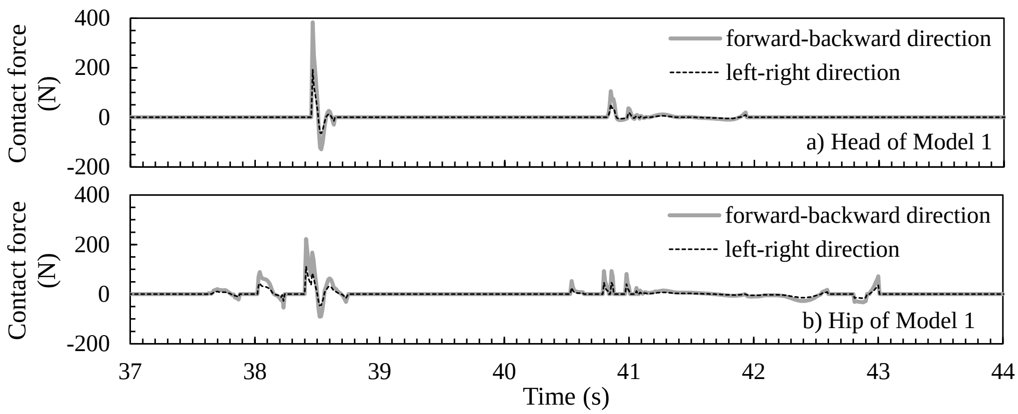

Figure 11. Time history of contact forces applied to model 1 near the time of collision (Case B)

The contact force between two models was generated between approximately 37 s and 44 s. The contact points were the head and hip. First, the hips of both models collided with each other, then the heads of both models collided. As shown in figure 10, Model 2 collided with Model 1 from a backward oblique direction, so the contact force applied to both the head and the hip was larger in the forward-backward direction than in the left-right direction. Therefore, as shown in figure 10, both models exhibited significant deviations in their posture, primarily in the forward-backward direction after the collision. As shown in figure 11, the maximum contact forces applied to the head and hip in the forward-backward direction are 383 N and 222 N, respectively. In the Case B, the two models collided while walking in the same direction, similar to an actual evacuation. In the Case A, on the other hand, the situation is equivalent to a head-on collision. Therefore, the contact forces in the Case B are smaller than in Case A. The contact forces in the Case B showed good agreement with those of previous study (Tamagawa, et al. (2011)). Therefore, the validity of the human body model considering collision constructed in this study is demonstrated.

CONCLUSION

In this study, in order to evaluate the human damage due to collision during an earthquake, the DEM was incorporated into the human body model. In order to investigate the validity of the model, we perform simulation of collision. The contact forces of the model constructed in this study showed good agreement with those of previous study (Tamagawa, et al. (2011)). Therefore, the validity of the human body model considering collision constructed in this study is demonstrated.

ACKNOWLEDGEMENT

Observation records were made publicly available by the Japan Meteorological Agency. We would like to express our gratitude for their cooperation.

REFERENCES

D. Gordon E. Robertson, Graham E. Caldwell, Joseph Hamill, Gary Kamen, and Saunders N. Whittlesey (2013). *Research Methods in BIOMECHANICS SECOND EDITION*, Human Kinetics

Hida Takenori, Itoi Tatsuya, and Takada Tsuyoshi (2019). “Development of Seismic Counter Measures Against Cliff Edges for Enhancement of Comprehensive Safety of Nuclear Power Plants -Part 11 Cliff Edges of Human Body Against Strong Shaking-,” 25th Conference on Structural Mechanics in Reactor Technology, Charlotte, NC, USA, August 4-9, 2019.

Ikuta Eisuke, Miyano Michio, Itoigawa Eiichi, Nishimura Akiyoshi, Tanaka Hiroshi, Kajiwara Kouichi, and Kumagai Yoshio (2005). “Analysis on the Mechanism of Human Casualties due to the 1995 Hyogoken-Nanbu Earthquake Based on the Comprehensive Database,” Journal of Architecture and Planning (Transactions of AIJ), No.590, pp.117-123, 2005. 4 (in Japanese)

Japan Meteorological Agency (2011). https://www.data.jma.go.jp/eqev/data/kyoshin/jishin/110311_tohokuchiho-taiheiyouoki/index.html (accessed 31. 3. 2025)

Kiyono Junji, Miura Fusanori, and Yagi Hiroaki (1998). “Simulation of Evacuation Behavior in a Disaster by Distinct Element Method,” Japanese Journal of JSCE, No.591/ I-43, 365-378, 1998. 4 (in Japanese)

Kouchi Makiko and Mochimaru Masaaki, 2005: AIST Anthropometric Database, National Institute of Advanced Industrial Science and Technology, H16PRO 287. https://www.airc.aist.go.jp/dhrt/91-92/index.html (accessed 31. 3. 2025)

National Research Institute of Fire and Disaster: Survey Report on Damages and Fire-fighting Activities of the 2004 Niigata Prefecture Chuetsu Earthquake, Research materials of NRIFD, No.69, 2005. 9 (in Japanese)

Sakuma Haruki and Hida Takenori (2023). "Evaluation of Evacuation Possibility During Earthquake based on Seismic Response Analysis Model of Human Body Considering Walking and Falling," EURODYN 2023 XII International Conference on Structural Dynamics, July 2023, Delft, The Netherlands.

Sato Takumi and Hida Takenori (2024). "Crowd Evacuation Simulation During Earthquake Using Seismic Response Analysis Models of Human Body," 18th World Conference on Earthquake Engineering, Milan, Italy, 30th June-5th July, 2024.

Takada Tsuyoshi, Itoi Tatsuya, Hida Takenori, Muramatsu Ken, Muta Hitoshi, Furuya Osamu, Minagawa Keisuke, Yamano Hidemasa, and Nishida Akemi (2017). "Development of Seismic Countermeasures Against Cliff Edges for Enhancement of Comprehensive Safety of NPPs – Part 1: Conceptual Study on Identification and Avoidance of Cliff Edges of NPPs Against Earthquakes," 24th Conference on Structural Mechanics in Reactor Technology, BEXCO, Busan, Korea, August 20-25, 2017.

Tamagawa Masaaki, Matsuura Hiroyuki, Nakano Masahiro, Yukimasa Toru, Yamanaka Makoto, and Kubota Masami (2011). "Fundamental Studies of Safety Assessment for Collision and Fall induced Human Injury 1st report, Understanding of Fundamental Phenomena in Dummy by Collision and Fall," Journal of Biomedical Fuzzy Systems Association, Vol.13, No.2, pp.97-104 (2011) (in Japanese)